

## Switching of vertical giant magnetoresistance devices by current through the device

K. Bussmann,<sup>a)</sup> G. A. Prinz, and S.-F. Cheng  
*Naval Research Laboratory, Washington, DC 20375*

D. Wang  
*Nonvolatile Electronics, Inc., Eden Prairie, Minnesota 55344*

(Received 1 June 1999; accepted for publication 23 August 1999)

Experiments are reported that demonstrate current-perpendicular-to-the-plane giant magnetoresistance devices can be switched repeatedly between the high- and low-resistance states by passing current vertically through the structure. The lithographically patterned devices, having diameters in the range of 0.3–0.7  $\mu\text{m}$ , operate at room temperature and exhibit distinctly separate switching of the soft and hard layers. Designs for magnetoelectronic random access memory can utilize this scheme for storing and reading information. © 1999 American Institute of Physics. [S0003-6951(99)04642-2]

Since the discovery of the giant magnetoresistance (GMR) effect in 1988,<sup>1</sup> there have been several successful technological applications including field sensors<sup>2</sup> and recording read heads,<sup>3</sup> as well as the demonstration of elements for random access memory (RAM).<sup>4</sup> All of these applications exploit the current-in-plane (CIP) GMR effect in which the current used to sense the magnetoresistance is propagated parallel to the interfaces of the multilayered planar structure. An alternative approach that propagates the current perpendicular to the planes (CPP) was first demonstrated in 1991 (Ref. 5) and showed a GMR effect some five times larger than the CIP effect for a similarly structured magnetic metal multilayer. Application of the CPP-GMR effect, which we shall refer to as vertical GMR devices, is much more challenging since the vertical devices have very low resistance unless they are fabricated to have small cross-sectional areas. No applications have yet been reported for vertical GMR devices.

Although there have been reports<sup>6,7</sup> of the effects of driving current through magnetic multilayers, in this letter we report experiments that demonstrate vertical GMR devices can be switched between the high- and low-resistance states by passing current through the device. We interpret our results to indicate the hard and soft magnetic layers form circularly oriented magnetizations that can be switched between parallel and antiparallel helicity using the magnetic field generated by the current through the device. These results, obtained at room temperature on lithographically patterned devices, can be fruitfully applied to the development of vertical GMR devices in magnetoelectronic random access memory. We note particularly the control of the circular magnetization by current-through-device switching is unique to the CPP geometry and leads to a dipole-free magnetic-field configuration of the remanent device magnetization that allows for a more stable quiescent state relative to linearly polarized devices.

GMR structures were patterned from rf-diode sputtered

metal multilayers. The metal sequence for this work was Si/SiN/40 Ta/1500 Cu/7 Ta/20 Cu/(23 NiFeCo/40 Cu/12 NiFe/40 Cu)<sub>5</sub>/1000 Cu/1500 SiN (thickness units are Å). The base SiN (silicon nitride) is grown by low-pressure chemical-vapor deposition on (100) Si wafers. The capping nitride serves as a protective layer and as a subsequent hard mask. It is deposited using reactive sputtering of Si in an Ar/N<sub>2</sub> atmosphere. Ta is used as both an adhesion layer and as a phase-breaking layer that reduces the grain size of the magnetic metals. Small grain-size materials reduce the influence of magnetocrystalline anisotropy allowing lower coercive fields to be obtained on unpatterned films.<sup>8</sup>

Devices were patterned using the process flow shown in Fig. 1. The metallized wafer is first patterned to the device level with optical lithography to a minimum feature size of 0.6  $\mu\text{m}$  using a mid-UV contact printer. CF<sub>4</sub>/4% O<sub>2</sub> reactive ion etching (RIE) followed by a photoresist strip in acetone defines the hard mask features in the top nitride. Electron-beam lithography using polymethyl methacrylate (PMMA) combined with a second RIE is used to reduce the size of the optically defined features to below 0.6  $\mu\text{m}$ . Following an

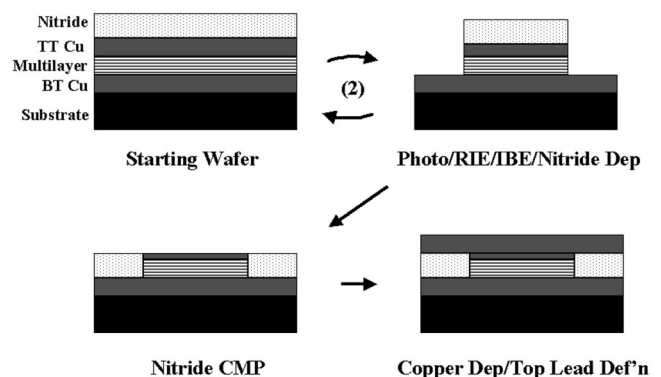


FIG. 1. Process flow for fabrication of vertical GMR devices. The abbreviations are defined as: top terminal copper (TTCu); bottom terminal copper (BTCu); photolithography/reactive ion etch/ion-beam etch/silicon nitride deposition (Photo/RIE/IBE/Nitride Dep); silicon nitride chemical-mechanical polishing (Nitride CMP); copper deposition/top lead definition (Copper Dep/Top Lead Def'n).

<sup>a)</sup>Electronic mail: bussmann@anvil.nrl.navy.mil

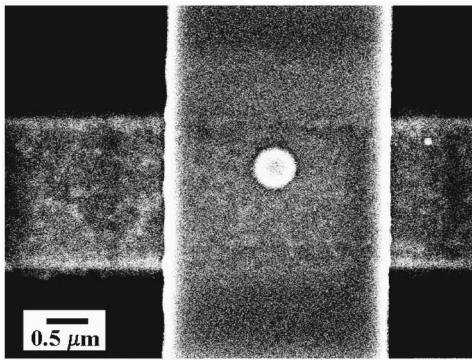


FIG. 2. Scanning electron micrograph of partially finished device structure immediately following the CMP step to expose the Cu top of the device. The BT line runs vertically in the image. The horizontal buried metal line is not functional.

acetone strip of the PMMA, the wafers are subjected to ion-beam etching [(IBE) 500 V/150 mA/8 cm DIA source] on a cooled stage to the bottom terminal (BT) level. The wafer is coated with nitride and subjected to a second sequence of optical lithography and IBE to define the BT layer. A thick nitride layer is grown and the wafer is subjected to chemical-mechanical polishing (CMP) of the nitride to open up the top of the devices. The wafer is passivated with benzotriazole (1 min in 0.4% BTA, by weight, in water) immediately after CMP and placed in a sputter deposition chamber where they are backsputtered in Ar:2.5% H<sub>2</sub> atmosphere before deposition of 1500 Å of copper and 1000 Å nitride. The lithographic process with IBE is repeated to define the top terminal (TT). A scanning electron microscopy (SEM) micrograph is shown in Fig. 2 of a patterned device immediately after the CMP step. The BT leads are the vertical leads and are above an electrically isolated and nonfunctional buried metal line running horizontal across the image. The BT and TT leads are nominally 3 μm wide.

Figure 3 shows the experimental configuration of our measurements. Wafers are mounted on a probe station and connected so that current runs in a hairpin geometry from the top-left to the bottom-left leads. Voltage is measured as the difference of the top-right and bottom-right leads. Measurements are made using a dc current source (Keithley model 236) and nanovoltmeter (Keithley model 182) and we define the hairpin resistance as  $V/I$  as measured by these instruments.

It is known from previous work that severe current density distributions can exist in this configuration. We and others<sup>9,10</sup> have shown the effect leads to an amplification of the apparent magnetoresistance caused by the exponential dependence of the measured voltage on the device resistivity. Though determination of the intrinsic resistivity change as a function of magnetic field is best handled by finite-element

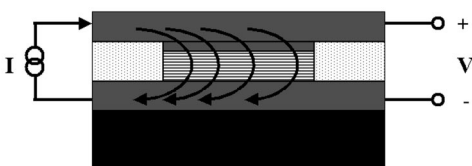


FIG. 3. Measurement setup and geometry used in determining device resistance.

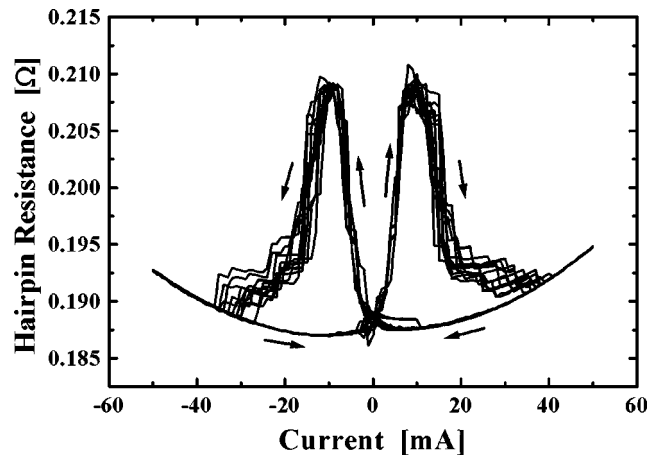


FIG. 4. Measured resistance of a multilayered device of 0.3 μm diam repeated ten times.

modeling, Lenczowski *et al.*<sup>11</sup> have developed a two-dimensional model that establishes a length scale  $\kappa$  in the exponential roll-off of the current density from the edge of the device to device center. For our devices and from measurements of the resistivity of the TT, device, and BT layers and their thicknesses,  $\kappa$  is estimated to be 0.23 μm. We, therefore, expect severe nonuniformities in the current distribution for the larger devices in this study. We are, however, able to interpret our results on the smallest device using a uniform current distribution model.

Figure 4 shows the results of repeated scans of current versus resistance applied to a 0.3-μm-diam device using the hairpin current configuration. Figure 4 represents ten scans performed consecutively on a single device. The most notable features are the significant resistance changes (~11%) seen as the current sweeps from the upper- and lower-current limits in a manner resembling the magnetization versus applied field loop of a magnetic sample. The parabolic background is due to heating effects that increase the device resistance with temperature. If we assume uniform current density, the maximum current applied to this structure corresponds to a current density of  $7 \times 10^7$  A/cm<sup>2</sup>. This value is large, though even higher applications of current failed to cause burnout of this device, indicating their robust structural qualities.

We interpret the changes in resistance as due to the re-orientation of the magnetization configuration in the multilayer device caused by the rotational field generated by the current passing through the device. The field generated from a uniform current density through a cylinder of radius  $r_0$  is along the azimuthal direction and easily calculated from Ampere's Law to have the radial dependence given by  $B_\phi = 2\pi \times 10^{-5} Jr$  for  $0 < r < r_0$  and  $B_\phi = 2\pi \times 10^{-5} Jr_0^2/r$  for  $r > r_0$ . (Note units of  $B_\phi$ ,  $J$ , and  $r$  are Oe, A/cm<sup>2</sup>, and μm, respectively.) For the device of Fig. 4 we determine the field at the outer edge of the device, for a drive current of 50 mA, to be 670 Oe. Such a field is strong enough to rotate the magnetization of the device in the outer region. Exchange coupling within each layer acts to pull the inner region of the device to form a circularly polarized orientation of the magnetization.

Discrimination between the hard and soft layers in switching is determined primarily by the thickness difference

of the layers and to the influence of edge poles that form during the switching process. At these dimensions and for the low intrinsic coercive fields of these materials, the switching process is driven by the dynamics of edge poles formed as the magnetization rotates in the plane of the film. By virtue of the reduced pole density, the thin magnetic layers will switch orientation prior to the thick layers and will act as the soft magnetic layers. The circular geometry, also a strong influence on the quiescent state magnetization at these dimensions, acts in concert with the applied field to stabilize the circular magnetic configuration. As seen in Fig. 4, if all of the layers initially have their magnetization vectors parallel, the device will be in the low-resistance GMR state and the first reversals are experienced by the soft (thin) layers when the device switches to the high-resistance antiparallel GMR state. For higher current, the increased induced field reverses the hard (thick) layers, and the device returns to the low-resistance GMR state with the magnetization vectors of all the magnetic layers parallel. As Fig. 4 shows, it is possible to switch these layers repeatedly between the high- and low-resistance states with nominal currents. The stability of the magnetization helicity is seen in the lack of resistance increase following saturation and return to zero applied current.

Although there is some variation in the magnitude of the resistance values seen in these scans, it is important to observe that the onset of the low-field switching of the soft layers occurs at  $\sim 4$  mA and the high-field switching of the hard layers occurs at  $\sim 15$  mA. These are current levels easily handled by the addressing circuits in present RAM technology. The variation in the resistance values themselves, we believe, arises from micromagnetic issues of the repeatability

in the distribution of the magnetization within the individual layers during the switching process. This issue must be addressed to bring the variation within acceptable limits.

In conclusion, we have fabricated cylindrical vertical GMR multilayer devices in the range of  $0.3\text{--}0.7\ \mu\text{m}$  in diameter and shown that they are capable of repeated switching at room temperature by passing currents directly through the devices. These devices, when assembled into a suitable memory matrix architecture, would serve as a basis for the development of a very high-density nonvolatile random access memory.

This work was supported by the Office of Naval Research.

- <sup>1</sup>M. Baibich, J. Broto, A. Fert, F. Nguyen Van Dau, F. Petroff, P. Etienne, G. Creuzet, A. Friederich, and J. Chazelas, *Phys. Rev. Lett.* **61**, 2472 (1988).
- <sup>2</sup>J. M. Daughton, J. Brown, E. Chen, R. Beech, A. Pohm, and W. Kude, *IEEE Trans. Magn.* **30**, 4608 (1994).
- <sup>3</sup>C. Tang, R. Fontana, T. Lin, D. E. Heim, V. S. Speriosu, B. A. Gurney, and M. L. Williams, *IEEE Trans. Magn.* **30**, 3801 (1994).
- <sup>4</sup>M. Dax, *Semicond. Int.* **20**, 84 (1997).
- <sup>5</sup>W. P. Pratt, Jr., S. F. Lee, J. M. Slaughter, R. Lolee, P. A. Schroeder, and J. Bass, *Phys. Rev. Lett.* **66**, 3060 (1991).
- <sup>6</sup>M. Tsoi, A. G. M. Jansen, J. Bass, W.-C. Chiang, M. Seck, V. Tsoi, and P. Wyder, *Phys. Rev. Lett.* **80**, 4281 (1998).
- <sup>7</sup>J. Z. Sun, *J. Magn. Magn. Mater.* **202**, 157 (1999).
- <sup>8</sup>P. Lubitz, S.-F. Cheng, K. Bussmann, G. A. Prinz, J. J. Krebs, J. M. Daughton, and D. Wang, *J. Appl. Phys.* **85**, 5027 (1999).
- <sup>9</sup>K. Bussmann, S. F. Cheng, G. A. Prinz, Y. Hu, R. Gutmann, D. Wang, R. Beech, and J. Zhu, *IEEE Trans. Magn.* **34**, 924 (1998).
- <sup>10</sup>R. J. M. van de Veerdonk, J. Nowak, R. Meservey, J. S. Moodera, and W. J. M. de Jonge, *Appl. Phys. Lett.* **71**, 2839 (1997).
- <sup>11</sup>S. K. J. Lenczowski, R. J. M. van de Veerdonk, M. A. M. Gijis, J. B. Giesbers, and H. H. J. M. Janssen, *J. Appl. Phys.* **75**, 5154 (1994).